

A Dynamic Nuclear Polarization spectrometer at 95 GHz/144 MHz with EPR and NMR excitation and detection capabilities

Akiva Feintuch^{a,*}, Daphna Shimon^a, Yonatan Hovav^a, Debamalya Banerjee^a, Ilia Kaminker^a, Yaacov Lipkin^a, Koby Zibzener^a, Boris Epel^b, Shimon Vega^a, Daniella Goldfarb^a

^a Department of Chemical Physics, Weizmann Institute of Science, Rehovot 76100, Israel

^b Department of Radiation & Cellular Oncology, MC1105, The University of Chicago Medical Center, Chicago, IL 60637, USA

ARTICLE INFO

Article history:

Received 22 July 2010

Revised 6 December 2010

Available online 1 January 2011

Keywords:

Dynamic Nuclear Polarization

W-band pulse EPR

EPR cavity

ABSTRACT

A spectrometer specifically designed for systematic studies of the spin dynamics underlying Dynamic Nuclear Polarization (DNP) in solids at low temperatures is described. The spectrometer functions as a fully operational NMR spectrometer (144 MHz) and pulse EPR spectrometer (95 GHz) with a microwave (MW) power of up to 300 mW at the sample position, generating a MW B_1 field as high as 800 KHz. The combined NMR/EPR probe comprises of an open-structure horn-reflector configuration that functions as a low Q EPR cavity and an RF coil that can accommodate a 30–50 μ l sample tube. The performance of the spectrometer is demonstrated through some basic pulsed EPR experiments, such as echo-detected EPR, saturation recovery and nutation measurements, that enable quantification of the actual intensity of MW irradiation at the position of the sample. In addition, DNP enhanced NMR signals of samples containing TEMPO and trityl are followed as a function of the MW frequency. Buildup curves of the nuclear polarization are recorded as a function of the microwave irradiation time period at different temperatures and for different MW powers.

© 2011 Elsevier Inc. All rights reserved.

1. Introduction

In the past few years Dynamic Nuclear Polarization (DNP) has become a highly attractive method for enhancing the sensitivity of NMR and MRI signals at commonly used high magnetic fields. The DNP phenomenon has been known since the discovery of the Overhauser effect [1,2] in the early 1950's, and has been discussed and applied extensively as described in numerous reviews (a partial list of Refs. [3–6]). DNP is most efficient at relatively low magnetic fields and therefore the rapid increase in the magnetic field strength used in modern NMR has led to a decline in the applications and interest in DNP. However, Griffin and co-workers have consistently shown, starting at the early 1990s, that by increasing the microwave (MW) power DNP can be highly efficient for magic angle spinning (MAS) high field NMR at low temperatures [6–12]. These studies together with the introduction of dissolution-DNP by Golman and co-workers [13–15], have stimulated a renewed interest in DNP and numerous new applications of DNP to solid-state and liquid state NMR and MRI have started to emerge. Following these developments, commercial DNP systems have been designed for dissolution-DNP (Hypersense, Oxford Inc.) and for solid state MAS DNP NMR applications (Avance III, Bruker Inc.). Besides these

commercial spectrometers a number of research groups have developed different variations of homebuilt DNP systems [16–21]. Most of these DNP systems are NMR application oriented and are therefore designed with a minimal flexibility for performing EPR measurements necessary for optimization of the DNP process.

The DNP process in solids involves a transfer of spin polarization from highly polarized electrons to adjacent nuclei. This is typically done by MW irradiation of a frozen glass forming solution which includes free radicals that serve as electron-spin polarizers. Molecules with target nuclei for polarization are dissolved in the solvents and irradiation around the EPR spectrum of the radicals can result in an enhancement of the NMR signal of these target nuclei. A number of mechanisms have been distinguished that explain the enhancement in solid DNP, namely the Solid Effect (SE) [4,22,23], the Cross Effect (CE) [24,25], and Thermal Mixing (TM) [3,26,27], involving hyperfine interactions of nuclear spins to one, two or more coupled electron spins, respectively. These mechanisms have been used over the years to interpret experimental results [3,5,28,29]. However, there is still a need to extend the theoretical descriptions enabling quantitative predictions, particularly at high fields, and to facilitate the design of new DNP experiments.

The complexity of the polarization enhancement processes can be attributed to the large number of physical parameters which affect the final nuclear signal intensities. These include experimental

* Corresponding author. Fax: +972 89344123.

E-mail address: akiva.feintuch@weizmann.ac.il (A. Feintuch).

parameters that can be controlled such as the MW irradiation frequency, the MW power, the temperature, the concentration of the free radicals and the type of glass forming solvent. In addition, intrinsic sample parameters such as electron and nuclear spins relaxation times and the strength of the electron–nuclear hyperfine and electron–electron dipolar interactions have also a strong influence on the nuclear enhancement. The development and confirmation of any theoretical model, taking into account all these aspects, requires systematic experimental studies that can follow the influence of these parameters on the NMR signal enhancement. This would require a highly flexible DNP spectrometer with extended EPR and NMR capabilities including EPR and NMR detection.

A significant challenge in building a flexible DNP spectrometer with both EPR and NMR detection is finding a correct tradeoff between its EPR and NMR specifications. For an efficient transfer of the available MW power to the sample, transmission of the MW irradiation into a cylindrical cavity is the preferred setup [30]. In addition, the RF irradiation for nuclear spin manipulations and NMR detection needs to be transferred to an RF coil containing the sample. An elegant solution for combining 140 GHz EPR and NMR irradiation to the sample was previously suggested by Griffin and co-workers, who used the strip of the RF coil as the walls of the MW cavity [31]. This design exhibiting a quality factor Q of a few hundred for the MW cavity as well as a good tuning profile for the RF, was used to demonstrate proton DNP enhancement of up to 400 obtained via ^1H – ^{13}C cross polarization [26]. Their setup includes a field sweep apparatus which enables field dependent acquisition of DNP spectra. In this type of configuration the size of the sample is restricted due to the cavity and contains typically only a few micro-liters. Yanoni and co-workers [32] demonstrated the use of an open structure high- Q Fabry–Perot resonator with an RF coil in the open space of the resonator. This probe design is in practice only appropriate for lower MW frequencies (up to 40 GHz), where the dimensions of the resonator are large enough to situate a RF coil. Granwehr and Köckenberger [33] have recently reported on a 95 GHz DNP spectrometer with a probe structure with a very low Q with longitudinal EPR detection. Their setup was used for cross relaxation measurements by electron–electron double resonance (ELDOR) and saturation recovery EPR measurements. However, as they pointed out, this setup is appropriate mainly for temperatures of 1–2 K, where the electron spin-lattice relaxation time is on the order of a second.

Here we report the design and performance of a flexible DNP spectrometer operating at 95 GHz/144 MHz with both EPR and NMR capabilities targeted at studying the basic low temperature solid DNP mechanisms and developing new DNP methodologies. Our choice of frequency was driven by the availability of high quality MW components and, more importantly, solid state MW amplifiers with relatively high output powers and affordable prices. This of course was also compatible with our interests in spin physics mechanistic studies, and not in high sensitivity and high resolution NMR applications. Our system employs a low- Q resonator including a horn and a movable reflector, based on the design of Wind et al. [34]. This design leaves ample space for locating the RF coil and sample holder. This enables us to perform basic pulsed EPR measurements, such as electron spin nutation and relaxation experiments, and to acquire NMR signals from 30 to 50 μl samples.

2. The experimental setup

2.1. The DNP spectrometer

Here we present a full description of the design of our DNP spectrometer. The MW bridge of our setup is similar to the one re-

ported recently by Goldfarb and co-workers for their 95 GHz pulsed EPR spectrometer [35]. It is a homemade MW bridge built from commercially available 95 GHz components. The MW source is a computer controlled synthesizer operating at 7.3 GHz with a bandwidth of ± 0.1 GHz (Herley, CTI XS-7311). Its MW output is fed into a X13 multiplier (ELVA Inc.) with a bandwidth of ± 0.5 GHz resulting in an operation frequency of $94.9 \text{ GHz} \pm 0.5 \text{ GHz}$. The output of the multiplier passes through a digital phase modulator (0/180) and a fast remote controlled PIN-switch in order to generate phase-controlled pulses. These pulses are further pre-amplified and fed into a voltage-controlled variable PIN attenuator for power adjustment. The MW is then fed into a gated 23 dB solid-state amplifier (Quinstar Inc.) with a saturated power output (P_s) of 1 W and the out coming MW is sent to the circulator. The maximum power measured at the output of the circulator is ~ 600 mW which at the bottom of the waveguide, just before the sample, is reduced to ~ 300 mW.

The MW signal from the sample, after passing the circulator and a 95 GHz mixer (Quinstar Inc.), is fed to a DC video amplifier and then detected. A band-pass filter (BPF) with a frequency range of 95 ± 0.5 GHz is situated before the mixer and is the component with the narrowest frequency bandwidth in the MW bridge, still significantly broader than most DNP spectrometers. Unlike the Goldfarb bridge [30], we have at this stage implemented only a single MW channel. The bridge is controlled by a standard PC through the use of a Pulseblaster (SpinCore Inc.) PCI card with a temporal resolution of 5 ns. The card provides 21 TTL output channels enabling the control of the different components of the bridge. For signal detection a high speed PCI digitizer (Agilent Inc. U1070a) with a sampling rate of 400 Msamples/s is used. The Specman4EPR [36] software is used to control the position, duration, phase and amplitude of the MW pulses and the EPR signal acquisition.

For the excitation and detection of the NMR signals a commercial Apollo Windows-based console (Tecmag Inc., Houston Texas) with two RF channels operating between 2 and 500 MHz is used. This console is externally triggered by the EPR pulse programmer. RF transmitters, 800 W or 400 W, with a bandwidth of 10–310 MHz, (Dressler Inc.) are used to amplify the RF pulses coming from the Apollo system.

2.2. The combined NMR–EPR probe

A liquid helium cryostat (STVP-NMR Janis Inc.) with an adjustable temperature ranging between 2.5 K and 80 K was fitted into the bore of a 200 MHz Bruker NMR magnet with an inner diameter of 89 mm. The magnetic field was reset to ~ 3.35 T, corresponding to a free radical EPR resonance frequency of ~ 94.9 GHz and a proton Larmor frequency of ~ 144.1 MHz.

The probe setup, which is inserted into the cryostat, is similar to the design used in the W-band pulse EPR spectrometer at the Weizmann Institute [37] and consists of two parts. The inner part remains inside the cryostat and consists of a waveguide connecting the MW bridge to the MW horn-antenna sitting at the bottom of the cryostat (see below). An oversized waveguide of a length of about 1 m is used to reduce MW power losses. The losses from the output of the circulator to the entrance of the horn were measured to be 3–4 dB resulting in a maximal power of ~ 300 mW at the horn. The other part of the probe, consists of the RF coil with a sample holder and the EPR reflector tuning mechanism. It can easily be removed from the cryostat for the replacement of samples while keeping the cryostat at low temperatures. The bottom part of the combined probe is shown in Fig. 1a. The horn-reflector setup is employed for MW excitation and detection. An aluminum rectangular homemade horn-antenna was used with inner dimensions similar to the standard gain antennas manufactured by Quinstar Inc. (Fig. 1b). The original Quinstar horn was not appropriate

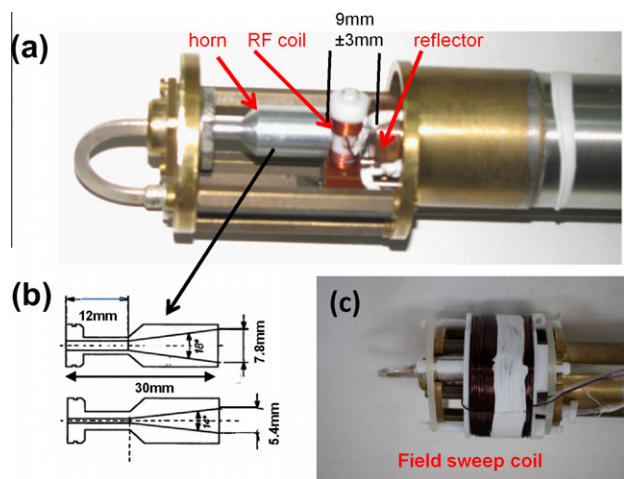


Fig. 1. (a) A photograph of the bottom part of the NMR-EPR probe. The positions both of the sample holder and the mirror can be controlled from outside the cryostat. (b) Sketches of the horn, showing a center cut from two perpendicular directions. (c) A photograph of the homemade sweep coil used for measuring the echo-detected EPR line.

because it contained magnetic material, affecting the homogeneity of the B_0 field and thus broadening the NMR lines. For the mirror a flat aluminum disc of 16 mm diameter was used. The distance between the mirror and the horn can be adjusted between 6 mm and 12 mm by moving the reflector from the outside of the cryostat. The RF coil is wrapped on a Teflon cylinder positioned in the gap between the horn and the mirror, which is also used to hold the sample. The position of this cylinder is adjustable as well.

The sample temperature is controlled via the temperature controller of the cryostat. An additional sensor is positioned on the waveguide insert 5–10 mm above the position of the sample. Experiments are performed only after stabilization of this sensor and the cryostat sensor (± 0.1 K) with a temperature gradient between the two sensors not greater than 1 K at low temperatures. Heating of a few tenths of a degree were measured on the top sensor during MW irradiation.

A homemade magnetic field sweep coil was added to the probe as implemented recently on the W-band pulse EPR spectrometer at the Weizmann Institute [38]. In our setup this coil is used to record echo detection (ED) EPR spectra of the radicals. Measuring an EPR spectrum using a field sweep is preferred over frequency dependent measurements, because the phase of the echo varies with frequency and a computer controlled phase correction is currently not possible due to the absence of quadrature detection capabilities. Optimization of the phase of the detected echo at each frequency can be done manually by a phase shifter positioned at the entrance to the mixer. The copper wire solenoid coil is mounted on the waveguide insert (see Fig. 1c) and is connected to a manually controlled DC current supply with a range of ± 10 A, providing a field sweep range of ± 18 mT. The frequency of the proton NMR signal was used to calibrate the field. Thus the ED-EPR spectra are measured at a constant frequency while varying current in the coil. At high currents some heating, of 1–5 K, is detected at the top temperature sensor close to the sample. This temperature change was corrected by readjusting the temperature at the bottom sensor for different currents so that the top sensor maintains a constant temperature throughout the measurement. The solenoid was only used for the ED-EPR spectrum measurements. All frequency dependent DNP enhancement experiments were obtained by varying the MW frequency.

For all NMR data shown here a single frequency RF tuning-matching circuit was used. A Helmholtz RF coil wrapped around

the two edges of the Teflon sample holder (Fig. 1a) enables a uniform penetration of the MW irradiation to the sample located in the space between the wires of the coil. The tunable capacitors of the RF circuit are located at the top of the cryostat and are connected to the coil via a solid coaxial cable. At the proton frequency the length of a 90° pulse is ~ 3 μ s and the ratio between the reflected and forward RF intensity of the RF circuit is about 20.

3. Results and discussion

In this section we show some of the features of the DNP spectrometer, especially in terms of EPR capabilities as well as DNP induced NMR enhancement measurements. Two samples were used for demonstrating the performance of this spectrometer (i) 15 mM trityl radical (OX063, GE Healthcare, AS) dissolved in 60:40(weight) DMSO/H₂O and (ii) 40 mM 4-Hydroxy-TEMPO dissolved in 60:40(weight) DMSO/H₂O. DMSO was used to obtain glassy samples at low temperatures for a homogeneous distribution of the radicals. Solutions of ~ 30 μ l were inserted into a shortened 4 mm glass NMR tube, degassed and sealed.

3.1. EPR measurements

ED-EPR signals were detected using a $\alpha - \tau - \alpha - \tau$ -echo sequence. The flip angle α of the MW pulses was much smaller than 90° due to the relatively low power at the sample, and in order not to exceed the electron phase-memory time. The actual length of the pulses was optimized by maximizing the echo amplitude and was in the order of 200–400 ns and the echo delay times τ were chosen in the range of 300–800 ns. Echo signals were acquired by the digitizer and stored after typically 100–200 accumulations. Fig. 2 presents a typical echo profile preceded by the microwave pulses that leak through the protect-switch. For measuring the transmitted B_1 MW field at the sample, a standard nutation type sequence was used which includes an initial MW pulse with variable length, τ_p , followed by an echo detection sequence. Repetition times of 10–100 ms were used between echo detections, depending on the temperature. The oscillation of the echo amplitude determines the nutation frequency ν_1 and thus the MW field strength $B_1 = \nu_1/\gamma_e$. Nutation results from the TEMPO sample at 30 K are shown in Fig. 3a with an oscillation of ~ 1.2 μ s compatible with a power of ~ 830 KHz. The decay of the oscillations is due to the electron phase-memory time T_m , which for this sample due to the high radical concentration is ~ 300 ns (data not shown). Longer decay times can be found for the trityl sample as shown in Fig. 3b for two different power settings, yielding ν_1 values of ~ 350 KHz and ~ 220 KHz. For low powers where the nutation is

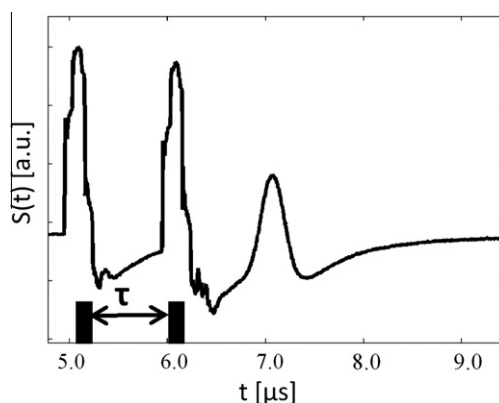


Fig. 2. A typical EPR echo from the TEMPO sample including the reflected MW pulses that leaked through the protect-switch (10 K).

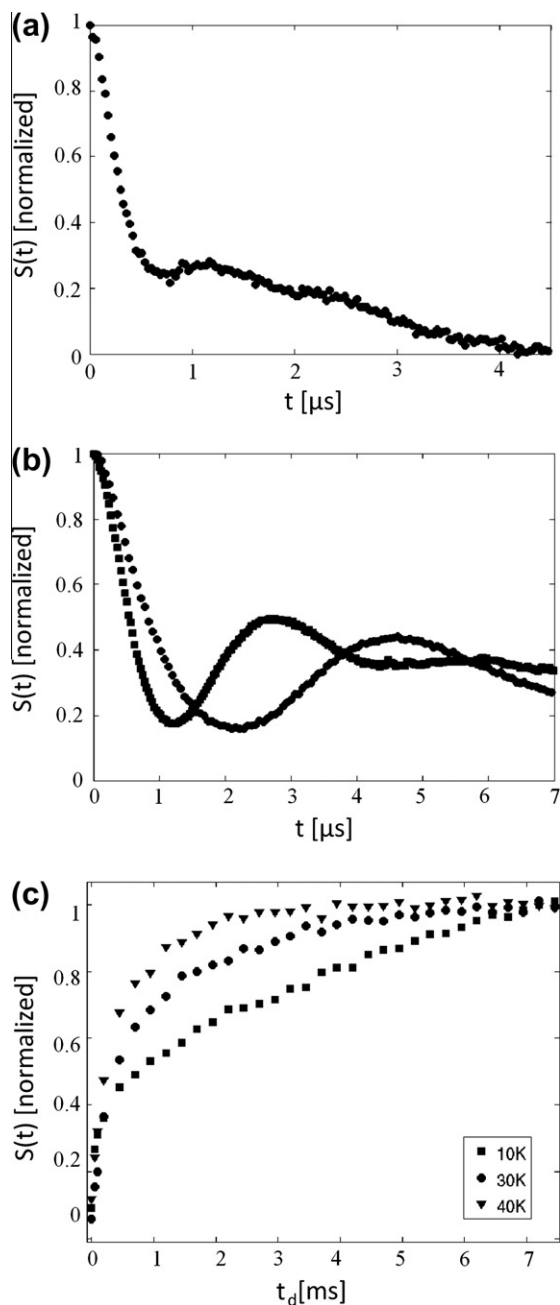


Fig. 3. (a) Nutation measurements on the TEMPO sample (30 K) yielding ~ 830 KHz. (b) Nutation measurements on the trityl sample for different powers (40 K) yielding 350 and 220 KHz. (c) Saturation recovery curves of the TEMPO sample measured at different temperatures.

not discernible due to the oscillation decay the power is calculated from a calibration chart based on power measurements at the output of the bridge.

Fig. 3c shows results of saturation recovery measurements on the TEMPO sample at different temperatures measured at the maximum echo intensity (at $B_0 = 3.385$ T). A saturation pulse of 50 ms was followed by a varying delay τ_d before an echo signal was detected. Here a repetition time of 60 ms was used. The recovery curves are characterized by two rate constants (see Table 1); the slow one corresponds to the electron spin-lattice relaxation time T_{1e} , while the fast one is due to spectral diffusion T_{SD} . T_{1e} and T_{SD} values for different temperatures are listed in Table 1.

The ED-EPR spectra (10 K) of the TEMPO and trityl samples obtained using the homemade sweep coil, are shown on the top panel

Table 1

Relaxation times obtained from exponential fits of the EPR saturation recovery measurements yielding T_{1e} and T_{SD} . The ^1H nuclear spin-lattice relaxation times were obtained from a saturation recovery experiment without MW. The DNP buildup were measured with our full MW power except for the power dependent measurements at 10 K which were done with the given values.

	T_{1e} (ms)	T_{SD} (ms)	T_{1n} (sec)	buildup (sec)
6 K	108	0.3	117	75
10 K	6	0.1	64	39 (800 KHz)
10 K	–	–	–	65 (225 KHz)
10 K	–	–	–	65 (150 KHz)
20 K	3.5	0.2	23	18
30 K	2	0.2	13	11.5
40 K	1	0.1	8	8.5
50 K	0.5	0.05	6	7.5

of Fig. 4. The trityl spectrum shows a singlet, with a FWHM of ~ 30 MHz a bit narrower than earlier reports in the literature [39]. The line shape of the spectrum of the TEMPO sample, however, is different from the classical powder pattern of nitroxides. In this spectrum the relative intensities of singularities corresponding to the A_{zz} features, as well as that of g_{xx} are enhanced compared to that of g_{yy} that is weak. This change is a consequence of the rather large concentration and long echo delay of $\tau = 800$ ns, which is longer than T_m . We attribute this severe distortion of the intensity profile of the ED-EPR to the anisotropy of the phase-memory time originating from spectral diffusion processes. Similar phenomena have been attributed to molecular librations occurring at low temperatures, leading to distortions of the powder pattern with increasing τ [40]. We have verified this experimentally and indeed the higher the concentration, the larger is the lineshape dependence on τ (data not shown).

3.2. NMR and DNP measurements

For the initial characterization of our DNP system we restricted ourselves to DNP-NMR measurements of protons. To simplify quantification, all measurements were performed without signal averaging. When necessary, the DNP enhanced proton signals were attenuated so as to stay inside the dynamic range of the analog-to-digital converter (ADC). The NMR signal intensities were obtained by measuring the echo intensity after a $90_x^0 - \tau - 90_{x/y}^0$ -echo sequence, with $\tau = 23$ μs and a pulse length of 3 μs , following the MW irradiation. The phase of the second pulse did not influence the polarization enhancement measurements. At each MW frequency a pre-saturation RF pulse of an intensity of 100 KHz was applied. This was followed by MW irradiation and proton echo signals were acquired immediately after the MW.

Fig. 4 shows the MW frequency dependent NMR signal enhancement, referred to as the DNP spectrum, for the TEMPO and trityl samples. For both samples the length of the MW irradiation pulse was 60 s. The enhancement values were obtained by dividing the DNP echo intensities by the thermal equilibrium echo intensity. In the DNP spectrum of the trityl the enhancement is rather low and the zero quantum and double quantum components of the DNP spectrum are separated from each other by twice the proton Larmor frequency (Fig. 4b, bottom), as expected from the SE mechanism and similar to earlier reports in the literature [41]. At the bottom of Fig. 4a we show the DNP spectrum of the TEMPO sample measured at 10 K. The broad spectral width of the MW bridge allowed us to measure the full DNP spectra covering ± 400 MHz without retuning of the probe. The DNP spectrum of the TEMPO sample is more complicated, and has previously been modeled based on the TM mechanism [25]. This result shows that the DNP spectrum is broader than the EPR spectrum indicating a contribution of the SE as well. This will be further discussed in a future publication.

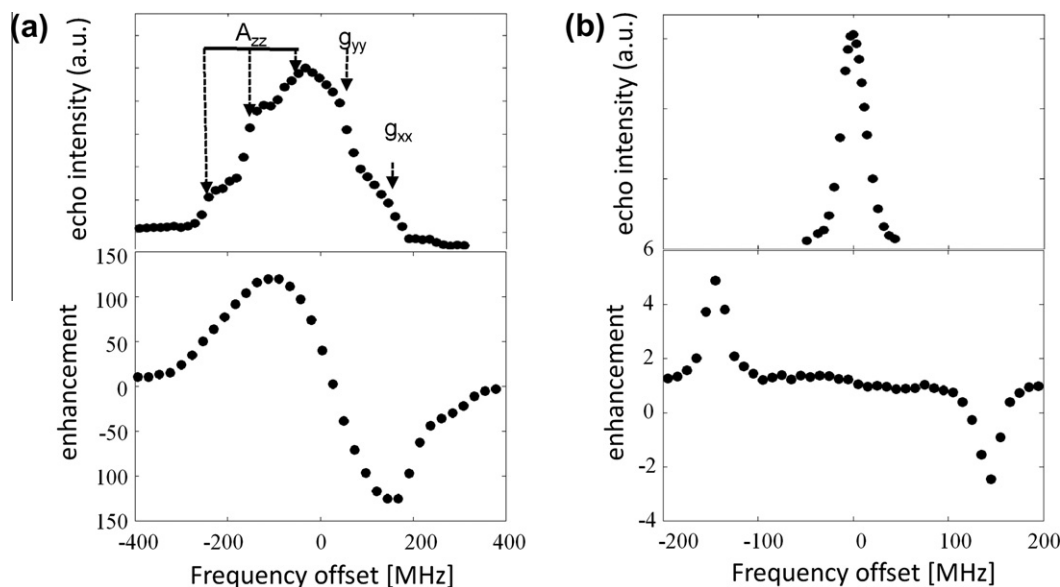


Fig. 4. (a) (top) ED-EPR spectrum of the TEMPO sample, and (bottom) the corresponding DNP spectrum (10 K). (b) The ED-EPR spectrum (top) and the corresponding DNP spectrum (bottom) for the trityl sample (40 K). In both cases the frequency scale is relative to $\nu = 95$ GHz.

Fig. 5a shows the proton signal enhancement (left scale) of the TEMPO sample as a function of the length of a MW pulse with an intensity of ~ 830 kHz, measured at 10 and 30 K (full circles and

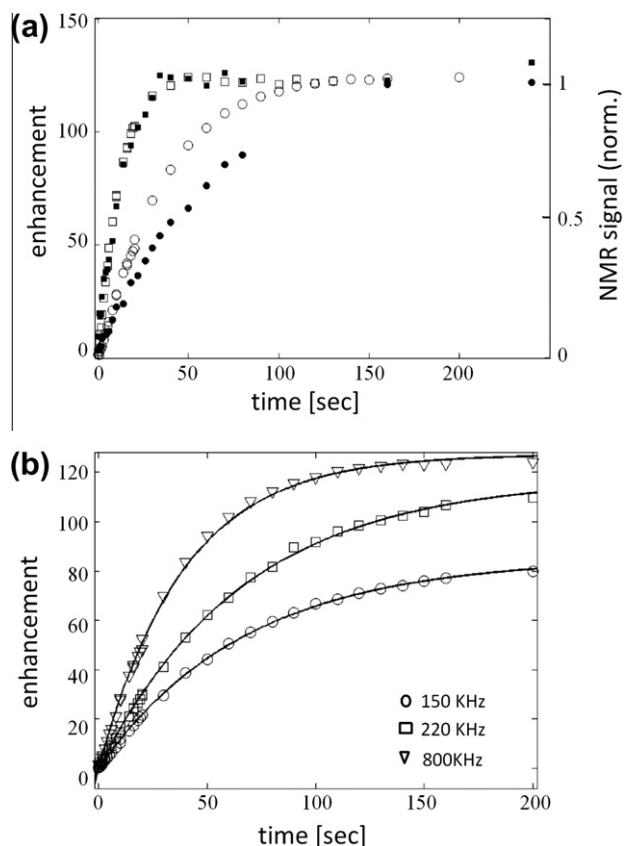


Fig. 5. Temporal dependence of the polarization buildup during DNP irradiation for the TEMPO sample. (a) Dependence of the buildup time on temperature (open circles (10 K) and squares (30 K), left scale). A saturation recovery experiment is also shown (full circles (10 K) and squares (30 K), right scale) for each temperature for comparing the two time constants. (b) Power dependence of buildup curves at 10 K for different MW powers ($B_1 = 800$ KHz, 225 KHz, 150 KHz) showing that T_{1n} is only an upper limit for the polarization time.

squares). The results of proton spin-lattice relaxation measurements (right scale) obtained by a saturation recovery sequence (no MW irradiation) at the same temperatures are presented on the same plot for comparison (open squares and circles). The fitted values of the buildup time constant and T_{1n} for different temperatures are listed in Table 1. At 30 K the DNP polarization buildup time is similar to T_{1n} , as has been demonstrated by others (see for example [16]). However, at 10 K the polarization buildup time is clearly shorter than T_{1n} .

The MW intensity (B_1) dependence of the DNP buildup profile of the TEMPO sample at 10 K is presented in Fig. 5b. The solid lines are least square fits of the data to a single exponent and the values obtained are listed in Table 1. For both of the low MW powers (225 KHz and 150 KHz) the fits result in the same buildup time of ~ 65 s. This time constant is very close to the T_{1n} value of ~ 64 s at 10 K, obtained by an exponential fit of a saturation recovery experiment (not shown). At the high MW power (~ 800 KHz) however the buildup time constant is much shorter than T_{1n} . These results could indicate that T_{1n} is an upper limit to the buildup time constants of the NMR signals. This type of observation was discussed in a recent study of the spin dynamics of model spin systems in the framework of SE-DNP [42,43]. This example illustrates the type of combined EPR and DNP measurements that can be carried out by the spectrometer and that in the future will form the foundation for the development of the theoretical approach and its verification. A systematic description and discussions of the experimental results obtained for different experimental conditions will be published separately.

4. Summary and conclusions

In this work we have described and demonstrated through some basic examples the construction and performance of our DNP spectrometer working at a MW frequency of 95 GHz. The main factors characterizing the system include its broad MW frequency irradiation bandwidth, its large operational temperature range, and its relatively high MW B_1 field that can reach up to 830 KHz. Additionally, we demonstrated its flexibility to perform pulse EPR experiments such as relaxation and nutation experiments, and NMR experiments on the same sample without changing its external parameters. We demonstrated that we can monitor

the different time constants of the DNP enhancement and the enhancement profiles as a function of frequency, calibrated MW intensity, temperature, and sample composition. All these parameters influence the different types of DNP processes and the spectrometer will enable us to quantify their influence experimentally in an effort to extend our understanding of the DNP-assisted polarization of the bulk nuclei in different samples.

Acknowledgments

We thank Alexey Potapov for help in setting up the EPR spectrometer. D.G. holds the Erich Klieger Chair in Chemical Physics. S.V. holds the Joseph and Marian Robbins Chair in Chemical Physics. This research is made in part possible by the historic generosity of the Harold Perlman Family.

References

- [1] A.W. Overhauser, *Phys. Rev.* 92 (1956) 411–415.
- [2] T.R. Carver, C.P. Slichter, *Phys. Rev.* 102 (1956) 975.
- [3] A. Abragam, M. Goldman, *Nuclear Magnetism: Order and Disorder*, Clarendon, Oxford, 1982.
- [4] C.D. Jeffries, *Dynamic Nuclear Orientation*, John Wiley, New York, 1963.
- [5] R.A. Wind, M.J. Duijvestijn, C. Van Der Lugt, A. Manenschijn, J. Vriend, *Progr. NMR Spectrom.* 17 (1985) 33–67.
- [6] T. Maly, G. Debelouchina, et al., *J. Chem. Phys.* 128 (2008) 052211.
- [7] L.R. Becerra, G.J. Gerfen, R.J. Temkin, D.J. Singel, R.G. Griffin, *Phys. Rev. Lett.* 22 (3561) (1993).
- [8] G.J. Gerfen, L.R. Becerra, D.A. Hall, R.G. Griffin, R.J. Temkin, D.J. Singel, *J. Chem. Phys.* 102 (1995) 9494–9497.
- [9] D.A. Hall, D.A. Maus, G.J. Gerfen, S.J. Inati, L.R. Becerra, F.W. Dahlquist, R.G. Griffin, *Science* 276 (1997) 930–932.
- [10] M. Rosay, A. Zeri, N.S. Astrof, S.J. Opella, J. Herzfeld, R.G. Griffin, *J. Am. Chem. Soc.* 123 (2001) 1010–1011.
- [11] M. Rosay, J.C. Lansing, K.C. Hadda, W.W. Bachovchin, J. Herzfeld, R.J. Temkin, R.G. Griffin, *J. Am. Chem. Soc.* 125 (2005) 13626–13627.
- [12] V.S. Bajaj, M.L. Mak-Jurkauskas, M. Belenky, J. Herzfeld, R.G. Griffin, *Proc. Natl. Acad. Sci.* 106 (2009) 9244–9249.
- [13] J.H. Ardenkjær-Larsen, B. Fridlund, A. Gram, G. Hansson, L. Hansson, M.H. Lerche, R. Servin, M. Thaning, K. Golman, *Proc. Natl. Acad. Sci. USA.* 100 (2003) 10158.
- [14] K. Golman, R. Zandt, M. Lerche, R. Pehrson, J.H. Ardenkjær-Larsen, *Cancer Res.* 66 (2006) 10855–10860.
- [15] S.E. Day, M.I. Kettunen, F.A. Gallagher, D. Hu, M. Lerche, J. Wolber, K. Golman, J.H. Ardenkjær-Larsen, K.M. Brindle, *Natl. Med.* 13 (2007) 1382–1387.
- [16] J. Leggett, R. Hunter, J. Granwehr, R. Panek, A.J. Perez-Linde, A.J. Horsewill, J. McMaster, G. Smith, W. Köckenberger, *Phys. Chem. Chem. Phys.* 12 (2010) 5883–5892.
- [17] J. Wolber, F. Ellner, B. Fridlund, A. Gram, H. Johannesson, G. Hansson, L.H. Hansson, M.H. Lerche, S. Mansson, R. Servin, M. Thaning, K. Golman, J.H. Ardenkjær-Larsen, *Nucl. Instrum. Methods Phys. Res., Sect. A* 526 (2004) 173–181.
- [18] A. Comment, B. van den Brandt, K. Uffmann, F. Kudzesau, S. Jannin, J.A. Konter, P. Hautle, W.T.H. Wenckebach, R. Gruetter, J.J. van der Klink, *Concepts Magn. Reson. Part B* 31 (2007) 255–269.
- [19] Robert I. Hunter, Paul A.S. Cruickshank, David R. Bolton, Peter C. Riedi, Graham M. Smith, *Phys. Chem. Chem. Phys.* 12 (2010) 5752–5756.
- [20] K.R. Thurber, W.M. Yau, R. Tycko, J. Magn. Reson. 204 (2010) 303–313.
- [21] Brandon D. Armstrong, Devin T. Edwards, Richard J. Wyde, Shamon A. Walker, Songi Han, *Phys. Chem. Chem. Phys.* 12 (2010) 5920–5926.
- [22] C. Jeffries, *Phys. Rev.* 106 (1967) 164–165.
- [23] A. Abragam, W.G. Proctor, *Comptes Rendus Hebdomadaires des Seances de l'Academie des Sciences* 246 (1958) 2253–2256.
- [24] C.F. Hwang, D.A. Hill, *Phys. Rev. Lett.* 19 (1967) 1011–1013.
- [25] D.S. Wollan, *Phys. Rev. B* 13 (1976) 3671–3685.
- [26] M. Borghini, *Phys. Rev. Lett.* 20 (1968) 419–421.
- [27] A. Abragam, M. Goldman, *Rep. Progr. Phys.* 41 (1978) 395–467.
- [28] D.S. Wollan, *Phys. Rev. B* 13 (1976) 3686–3696.
- [29] C.T. Farrar, D.A. Hall, G.J. Gerfen, S.J. Inati, R.G. Griffin, *J. Chem. Phys.* 114 (2001) 4922–4933.
- [30] C.P. Poole, *Electron Spin Resonance*, Wiley, New York, 1983.
- [31] V. Weis, M. Bennati, M. Rosay, J.A. Bryant, R.G. Griffin, *J. Magn. Reson.* 140 (1999) 293–299.
- [32] J. Singel, H. Seidel, R.D. Kendrick, C.S. Yannoni, *J. Magn. Reson.* 81 (1989) 145–161.
- [33] J. Granwehr, W. Köckenberger, *Appl. Magn. Reson.* 34 (2008) 355–378.
- [34] R.A. Wind, F.E. Anthonio, M.J. Duijvestijn, J. Smidt, J. Trommel, G.M.C. de Vette, *J. Magn. Reson.* 52 (1983) 424–434.
- [35] D. Goldfarb, Y. Lipkin, A. Potapov, Y. Gorodetsky, B. Epel, A.M. Raitsimring, M. Radoul, I. Kaminker, *J. Magn. Reson.* 194 (2008) 8–15.
- [36] B. Epel, I. Gromov, S. Stoll, A. Schweiger, D. Goldfarb, *Concepts Magn. Reson. B* 26 (2005) 36–45.
- [37] I. Gromov, V. Krymov, P. Manikandan, D. Arieli, D. Goldfarb, *J. Magn. Reson.* 139 (1999) 8–17.
- [38] I. Kaminker, A. Potapov, A. Feintuch, S. Vega, D. Goldfarb, *Phys. Chem. Chem. Phys.* 11 (2009) 6799–6806.
- [39] J.H. Ardenkjær-Larsen, S. Macholl, H. Jóhannesson, *Appl. Magn. Reson.* 34 (2007) 509–522.
- [40] E.G. Bagryanskaya, D.N. Polovyanenko, M.V. Fedin, L. Kulik, A. Schnegg, A. Savitsky, K. Möbius, A.W. Coleman, G.S. Ananchenko, J.A. Ripmeester, *Phys. Chem. Chem. Phys.* 11 (2009) 6700–6707.
- [41] K. Hu, V.S. Bajaj, M. Rosay, R.G. Griffin, *J. Chem. Phys.* 126 (2007) 044512.
- [42] Y. Hovav, A. Feintuch, S. Vega, *J. Magn. Reson.* 207 (2010) 176–189.
- [43] Y. Hovav, A. Feintuch, S. Vega, *J. Chem. Phys.*, in press. doi:10.1063/1.3526486.